LETTER

doi:10.1038/nature10546

Image-based genome-wide siRNA screen identifies selective autophagy factors

Anthony Orvedahl[1,2]*, Rhea Sumpter Jr[1,3]*, Guanghua Xiao[4], Aylwin Ng[5,6,7], Zhongju Zou[1,3,8], Yi Tang[9], Masahiro Narimatsu[10], Christopher Gilpin[11], Qihua Sun[1,3], Michael Roth[12,13], Christian V. Forst[4], Jeffrey L. Wrana[10,14], Ying E. Zhang[9], Katherine Luby-Phelps[11], Ramnik J. Xavier[5,6,7], Yang Xie[4,13] & Beth Levine[1,2,3,8,13]

Selective autophagy involves the recognition and targeting of specific cargo, such as damaged organelles, misfolded proteins, or invading pathogens for lysosomal destruction[1–4]. Yeast genetic screens have identified proteins required for different forms of selective autophagy, including cytoplasm-to-vacuole targeting, pexophagy and mitophagy, and mammalian genetic screens have identified proteins required for autophagy regulation[5]. However, there have been no systematic approaches to identify molecular determinants of selective autophagy in mammalian cells. Here, to identify mammalian genes required for selective autophagy, we performed a high-content, image-based, genome-wide small interfering RNA screen to detect genes required for the colocalization of Sindbis virus capsid protein with autophagolysosomes. We identified 141 candidate genes required for viral autophagy, which were enriched for cellular pathways related to messenger RNA processing, interferon signalling, vesicle trafficking, cytoskeletal motor function and metabolism. Ninety-six of these genes were also required for Parkin-mediated mitophagy, indicating that common molecular determinants may be involved in autophagic targeting of viral nucleocapsids and autophagic targeting of damaged mitochondria. Murine embryonic fibroblasts lacking one of these gene products, the C2-domain containing protein, SMURF1, are deficient in the autophagosomal targeting of Sindbis and herpes simplex viruses and in the clearance of damaged mitochondria. Moreover, SMURF1-deficient mice accumulate damaged mitochondria in the heart, brain and liver. Thus, our study identifies candidate determinants of selective autophagy, and defines SMURF1 as a newly recognized mediator of both viral autophagy and mitophagy.

To identify novel genes required for selective autophagy, we performed a genome-wide siRNA screen to detect changes in the colocalization of a red-labelled Sindbis virus (SIN) capsid protein with a green fluorescent protein (GFP)-labelled marker of autophagosomes, GFP–LC3 (LC3 is also known as MAP1LC3) (Supplementary Fig. 1a) in SIN-infected HeLa/GFP–LC3 cells (ref. 6). Using correlative light and electron microscopy, we confirmed that colocalized red and green puncta represented autophagic structures (primarily autolysosomes) containing numerous viral nucleocapsids (Fig. 1a). The predominance of viral nucleocapsids concentrated in these structures (relative to within the cytoplasm) is consistent with selective autophagic targeting of viral nucleocapsids (herein referred to as virophagy).

Screening of a human siGenome library containing 21,215 siRNA pools showed that knockdown of 195 and 13 genes resulted in decreased or increased colocalization, respectively, (Fig. 1b, Supplementary Table 1 and Supplementary Fig. 1b). Genes were re-screened with sets of four individual siRNAs (Supplementary Table 2; see column 'J' of Supplementary Table 3 for siRNA sequences) to confirm our primary screen and rule out potential off-target effects of individual siRNAs; knockdown with two or more siRNAs resulted in decreased colocalization for 141 (72%) genes. (Fig. 2 and Supplementary Figs 1b and 2a). None of these 141 gene knockdowns decreased numbers of green puncta in uninfected cells (data not shown), indicating that these genes function in virophagy, but not in regulation of autophagy. There was no enrichment of siRNAs-containing microRNA seed sequences among these genes ($P = 0.95$) (Supplementary Tables 3 and 4), indicating that bias due to miRNA-like off-target effects was unlikely. There was a low confirmation rate for siRNAs that increased colocalization (2 of 13 genes); therefore, we subsequently focused only on siRNAs that decreased colocalization.

Bioinformatic analyses of the 141 confirmed hits required for SIN capsid/GFP–LC3 colocalization showed enrichment for gene sets associated with biological processes and molecular functions including RNA splicing/processing, protein phosphorylation, transport, calcium-binding and the cytoskeleton (Supplementary Table 5 and Supplementary Fig. 3a). Examination of our hits within a framework of functional cellular pathways revealed strongly enriched network modules associated with RNA processing, interferon (IFN)-α and -γ signalling, SNARE vesicular transport, cytoskeletal-associated components, and several metabolic pathways (Supplementary Fig. 3b and Fig. 1c). This is consistent with the function of IFN-γ in selective microbial autophagy[1] and the described role of the actin cytoskeleton in selective autophagy in yeast[7] and mammalian[8] cells. The enrichment of SNARE proteins suggests that in addition to a function in autophagosome formation and maturation[9,10], these proteins may be involved in the trafficking of selective cargo to the autophagosome. Twelve colocalization hits form primary interactions with core autophagy machinery and associated components[11] (Fig. 1d). One colocalization screen hit, clathrin interaction 1 (CLINT) interacts with ATG8 components (GABARAPL1, MAP1LC3A, MAP1LC3B), which are crucial in the recognition of cargo during selective autophagy[2]. Another hit, ATG13, is a member of the core autophagy network, indicating that it may have an as yet undefined function in selective autophagy, in addition to its role in the ULK1 (also known as Atg1) autophagy induction complex[12]. Five colocalization hits, SMURF1, NEFM, KCNAB2, SFRS4 and UBA52, interact with p62 (also known as SQSTM1), a known adaptor in diverse

[1]Department of Internal Medicine, University of Texas Southwestern Medical Center, Dallas, Texas 75390-9113, USA. [2]Department of Microbiology, University of Texas Southwestern Medical Center, Dallas, Texas 75390-9113, USA. [3]Center for Autophagy Research, University of Texas Southwestern Medical Center, Dallas, Texas 75390-9113, USA. [4]Department of Clinical Sciences, University of Texas Southwestern Medical Center, Dallas, Texas 75390-9113, USA. [5]Center for Computational and Integrative Biology, Massachusetts General Hospital, Harvard Medical School, Boston, Massachusetts 02114, USA. [6]Gastrointestinal Unit, Massachusetts General Hospital, Harvard Medical School, Boston, Massachusetts 02114, USA. [7]Broad Institute of Harvard and Massachusetts Institute of Technology, Cambridge, Massachusetts 02142, USA. [8]Howard Hughes Medical Institute, University of Texas Southwestern Medical Center, Dallas, Texas 75390-9113, USA. [9]Laboratory of Cellular and Molecular Biology, Center for Cancer Research, National Cancer Institute, National Institutes of Health, Bethesda, Maryland 20892, USA. [10]Center for Systems Biology, Samuel Lunenfeld Research Institute, Mount Sinai Hospital, Toronto, Ontario M5G 1X5, Canada. [11]Department of Cell Biology, University of Texas Southwestern Medical Center, Dallas, Texas 75390-9113, USA. [12]Department of Biochemistry, University of Texas Southwestern Medical Center, Dallas, Texas 75390-9113, USA. [13]Harold C. Simmons Comprehensive Cancer Center, University of Texas Southwestern Medical Center, Dallas, Texas 75390-9113, USA. [14]Department of Molecular Genetics, University of Toronto, Toronto, Ontario M5S 3E1, Canada.
*These authors contributed equally to this work.

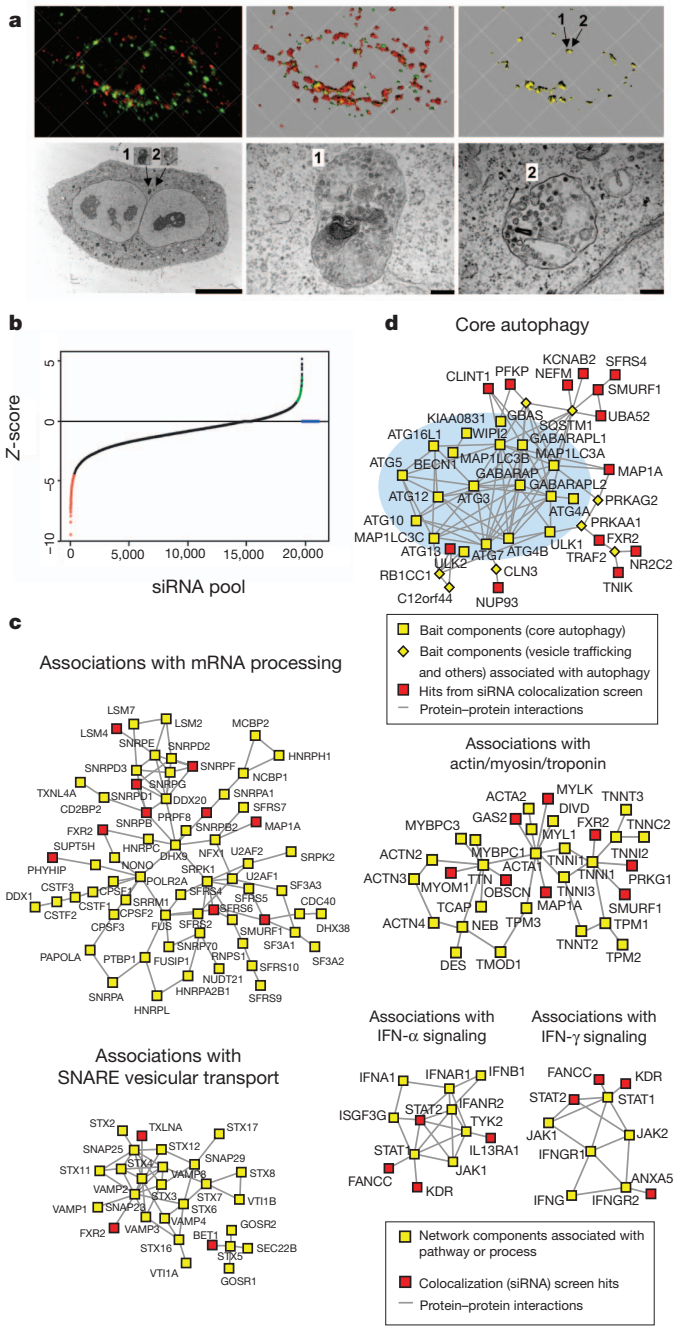

Figure 1 | Genome-wide screen to identify cellular factors required for Sindbis virus capsid colocalization with autophagosomes. **a**, Correlative light and electron microscopy of HeLa/GFP–LC3 cell infected with SIN/mCherry.capsid virus. Top left, deconvolved image of red and green fluorescence channels; middle, three-dimensional surface reconstruction of red and green channels; right, yellow (red + green) colocalization channel. Arrows denote yellow puncta that correspond to '1' and '2' in electron microscopy images below. Bottom left, electron microscopy of identical cell; middle and right, high magnification images of insets '1' and '2'. Scale bars, left, 10 μm; middle and right, 200 nm. **b**, Ranked distribution of median *Z*-scores for each siRNA pool in primary colocalization (virophagy) screen. Red, decreased colocalization; green, increased colocalization; blue, insufficient numbers of green or red puncta per cell or total number of cells per well for analysis. **c**, Maps of protein interactions in enriched network modules (see Supplementary Fig. 3b). **d**, Association of siRNA hits with autophagy network.

forms of selective autophagy[2], including SIN capsid targeting to autophagosomes[6].

Selective SIN autophagy (virophagy) promotes the survival of SIN-infected cells[6]. To determine if our identified candidate virophagy genes have a similar function, we screened our confirmation siRNA library for genes that decreased cell survival after SIN infection. Two or more siRNAs targeting 98 of the genes decreased cell survival after SIN infection (Fig. 2, Supplementary Tables 3 and 6 and Supplementary Figs 1b and 2a); colocalization and cell survival effects of individual siRNAs were significantly correlated (Supplementary Fig. 2b) ($P = 3.8 \times 10^{-8}$, Spearman correlation). This is consistent with a pro-survival function of autophagic targeting of SIN capsid in virally infected cells[6].

To investigate whether the identified candidate virophagy genes also function in other forms of selective autophagy, we performed a secondary screen for autophagy of damaged mitochondria (mitophagy). We used HeLa cells that express an mCherry fusion of Parkin, a cytosolic E3 ubiquitin ligase that translocates to depolarized mitochondria to induce mitophagy after treatment with uncoupling agents (such as CCCP, carbonyl cyanide *m*-chlorphenylhydrazone)[13]. Of the 141 confirmed colocalization hits, 2 or more siRNAs targeting 96 (68%) genes decreased mitophagy (Fig. 2, Supplementary Tables 3 and 7 and Supplementary Figs 1b and 2a, b). Host factors involved in viral autophagy and mitophagy overlapped significantly ($P = 0.019$, Spearman correlation). The minority of genes that only scored positive in either the virophagy confirmation or the mitophagy secondary screen may have a role in targeting some, but not other cargoes, for selective autophagy; however, the lack of overlap may also reflect different sensitivities of the two screens. Mitophagy hits consisted of several mitochondria-associated components[14] (NME2, MDH1, NTHL1, PDK1, COX8A, MRPS2, MRPS10, NDUFB9 and BLOC1S) and interactors of mitochondria-associated components (Supplementary Fig. 4).

We focused further on one gene, *SMURF1* (SMAD specific E3 ubiquitin protein ligase 1), encoding a HECT-domain ubiquitin ligase that targets several cytoplasmic proteins for degradation[15]. *SMURF1* was a confirmed hit in all three confirmation or secondary screening assays (see Supplementary Fig. 5 for representative raw data from colocalization confirmation screen), is present in two of the enriched networks (mRNA processing and actin cytoskeleton) (Fig. 1c), and is a predicted interacting partner of the autophagy adaptor, p62 (refs 2, 4, Fig. 1d).

We confirmed that SMURF1 is not required for general autophagy, but is a bona fide mediator of selective autophagy, including virophagy and mitophagy. siRNA knockdown of SMURF1 in HeLa cells, unlike knockdown of the essential autophagy protein, ATG7, did not alter general starvation-induced autophagy (Supplementary Fig. 6a). Furthermore, *Smurf1*$^{-/-}$ murine embryonic fibroblasts (MEFs) had normal levels of starvation-induced LC3-II (lipidated form of MAP1LC3) conversion, p62 degradation, and ultrastructural evidence of autophagosome and autolysosome accumulation (Fig. 3a, b).

However, a significant decrease in SIN/mCherry.capsid/GFP–LC3 colocalization was observed in SIN-infected *Smurf1*$^{-/-}$ MEFs (Fig. 3c, d). Similar to p62 (ref. 6), SMURF1 and SIN capsid protein co-immunoprecipitate in SIN-infected MEFs and HeLa cells (Supplementary Fig. 7a, b). SMURF1 is not required for the interaction between p62 and SIN capsid (Supplementary Fig. 7c). The interaction between SMURF1 and SIN capsid may be relevant for targeting SIN capsid for autophagosomal degradation, as levels of SIN capsid were increased in *Smurf1*$^{-/-}$ MEFs and *SMURF1* siRNA-treated HeLa cells. (Supplementary Fig. 7d–f). Increased SIN capsid levels in *Smurf1*-deficient cells cannot be explained by increased capsid production because viral growth was similar in *Smurf1*$^{-/-}$ and wild-type MEFs (Supplementary Fig. 7g, h), or by changes in proteasomal degradation because SIN capsid levels were not altered by treatment with the proteasome inhibitor MG132 (Supplementary Fig. 7d), and SIN capsid ubiquitination was not detected (data not shown). SIN-infected *Smurf1*$^{-/-}$ MEFs had accelerated cell death (despite similar viral titres) as compared to wild-type controls (Fig. 3g). Thus, SMURF1 interacts with SIN capsid, SMURF1 is required for SIN capsid

Gene symbol	C	S	M	Gene symbol	C	S	M	Gene symbol	C	S	M	Gene symbol	C	S	M	Gene symbol	C	S	M	Gene symbol	C	S	M	Gene symbol	C	S	M	Gene symbol	C	S	M
ACIN1	4	4	3	*CALCB*	0	1	3	*EIF2AK1*	2	0	1	*HIST1H3H*	3	2	0	*MAP1A*	3	2	4	*NR3C1*	0	0	1	*RGS17*	1	1	1	*STK32A*	4	0	2
ACTRT1	2	2	4	*CAPS*	2	0	2	*EIF2S1*	0	2	4	*HPR*	1	4	3	*MAP2K1*	3	0	4	*NTHL1*	2	3	4	*RIMS3*	2	0	4	*STOM*	2	4	2
ADAMTS7	3	1	3	*CCDC36*	4	3	1	*ENC1*	2	0	1	*HSF2BP*	2	1	3	*MAP3K12*	3	0	4	*NTN4*	2	1	1	*SATB1*	3	1	0	*STX10*	3	1	1
ADRB2	1	0	2	*CD163L1*	2	4	3	*FABP1*	0	4	2	*IL13RA1*	2	0	1	*MBD5*	4	4	2	*NUP93*	4	3	3	*SCN1A*	1	2	1	*SUPT3H*	3	2	3
AKR1E2	3	1	3	*CD93*	2	3	3	*FAM131B*	4	2	3	*IMP3*	3	1	0	*MDH1*	4	3	3	*OBSCN*	3	1	2	*SCRN1*	1	0	1	*TBC1D5*	1	1	4
ALKBH5	4	4	1	*CDK2AP1*	1	1	1	*FAM13B*	2	2	4	*IPPK*	3	0	4	*MEX3C*	2	1	2	*P2RX5*	2	2	3	*SERPINB10*	3	4	2	*TEAD4*	1	3	1
ALPK1	3	3	3	*CETN1*	2	1	0	*FAM176B*	1	0	2	*ITPKC*	1	2	3	*MLLT3*	3	1	1	*P2RY4*	1	0	0	*SFRP4*	4	0	3	*TMEM203*	2	4	2
ANXA5	3	3	2	*CHAF1B*	1	4	3	*FANCC*	3	0	3	*KCNAB2*	4	0	1	*MRPS10*	4	4	2	*PDK1*	1	1	4	*SFRS4*	2	0	1	*TMEM39A*	0	2	4
ASB2	3	4	4	*CHCHD8*	2	1	1	*FANCF*	4	1	2	*KCNH3*	0	0	1	*MRPS2*	3	2	3	*PDK4*	4	2	1	*SLC1A3*	2	4	3	*TMEM39B*	3	3	4
ATG13	2	1	2	*CHST3*	2	2	3	*FANCL*	2	4	1	*KCNK3*	2	0	4	*MS4A4A*	1	0	1	*PEX13*	2	3	3	*SLC1A4*	3	0	2	*TNIK*	2	2	0
ATP1B1	3	4	4	*CLDN7*	2	2	1	*FCGR3B*	1	2	4	*KCNQ1*	2	2	1	*MSTN*	3	3	3	*PEX3*	2	4	3	*SLC22A3*	1	0	3	*TREM1*	1	4	2
BET1	2	0	0	*CLINT1*	2	0	1	*FGF14*	3	4	0	*KDR*	3	1	0	*MTSS1*	1	2	1	*PFKP*	2	1	3	*SLC25A19*	3	3	0	*TRPC5*	3	0	0
BLOC1S1	0	0	2	*CLVS1*	1	1	2	*FGF7*	2	2	1	*KIAA0174*	1	3	2	*MYH11*	0	0	2	*PGK2*	2	1	4	*SLC25A36*	3	1	1	*TXLNA*	2	1	2
BMP2KL	4	2	2	*CNOT7*	1	0	1	*FGFBP1*	2	3	3	*KIAA0232*	0	0	0	*MYLK*	3	2	3	*PHYHIP*	3	3	3	*SLC35B3*	3	3	4	*UBA52*	2	2	1
BOC	3	1	2	*COX6B1*	1	1	1	*FLJ25363*	2	0	2	*KRCC1*	2	1	4	*MYLK3*	3	1	0	*PI4K2A*	2	1	2	*SLC35C1*	3	4	4	*YIPF1*	2	3	3
C11orf41	3	3	3	*COX8A*	0	3	4	*FXR2*	2	2	1	*KRT15*	1	1	2	*MYOM1*	4	3	4	*PIK3CA*	1	0	4	*SLC37A4*	3	3	2	*ZCCHC17*	2	3	3
C14orf104	4	3	2	*CPA3*	4	2	1	*GABRA5*	3	3	2	*KRT6A*	3	3	4	*NADSYN1*	2	0	1	*PLOD2*	1	1	3	*SLC6A1*	1	0	4	*ZFYVE16*	2	1	1
C1orf210	4	3	0	*CRNKL1*	2	3	3	*GAS2*	2	0	0	*KRT73*	2	1	3	*NAGA*	0	0	1	*PNPO*	2	4	4	*SLCO1A2*	1	1	2	*ZNF189*	1	3	2
C1orf223	2	4	2	*CSPG5*	4	4	2	*GDF5*	2	1	2	*LARP1B*	2	1	3	*NDUFA4L2*	1	1	0	*PPY*	3	4	2	*SMURF1*	2	2	2	*ZNF593*	2	1	4
C20orf12	1	1	2	*CXCR7*	0	4	1	*GMIP*	1	2	2	*LENG9*	1	3	3	*NDUFB9*	3	1	2	*PRKD2*	4	0	2	*SNRPB*	4	3	3	*ZNF681*	3	2	1
C3orf72	2	1	1	*DAAM2*	2	0	1	*GNE*	1	0	0	*LMCD1*	4	2	4	*NEFM*	3	0	2	*PRKG1*	2	0	2	*SNRPB2*	3	3	0				
C5	3	1	4	*DHX38*	1	1	0	*GPC1*	1	0	1	*LOC387849*	2	3	4	*NF2*	3	1	1	*RBM18*	1	3	0	*SNRPD1*	3	2	4				
C7orf68	2	2	1	*DKKL1*	4	3	2	*GPR81*	3	3	2	*LOC402210*	2	0	0	*NLRP14*	1	1	1	*RCTP1*	1	0	0	*SNRPF*	4	0	2				
C8orf59	3	2	2	*DPF3*	2	3	4	*HAPLN1*	2	1	2	*LRPAP1*	1	0	0	*NME2*	1	1	4	*REEP2*	4	2	1	*SNTG1*	0	2	2				
CA7	2	2	3	*DUSP22*	0	1	0	*HEATR6*	3	1	1	*LSM4*	4	4	3	*NR2C2*	2	1	4	*RFWD3*	4	3	2	*STAT2*	3	4	2				

Figure 2 | Gene list for viral capsid/autophagosome colocalization (C) confirmation screen and secondary screens for survival of virus-infected cells (S) and Parkin-mediated mitophagy (M). Shown are the numbers of individual siRNAs from a pool of four targeting each gene that scored positive in each screen. Red, genes with 2 or more positive siRNAs (confirmed hits); Green, genes with <2 positive siRNAs. See Supplementary Tables 2–8 for further details.

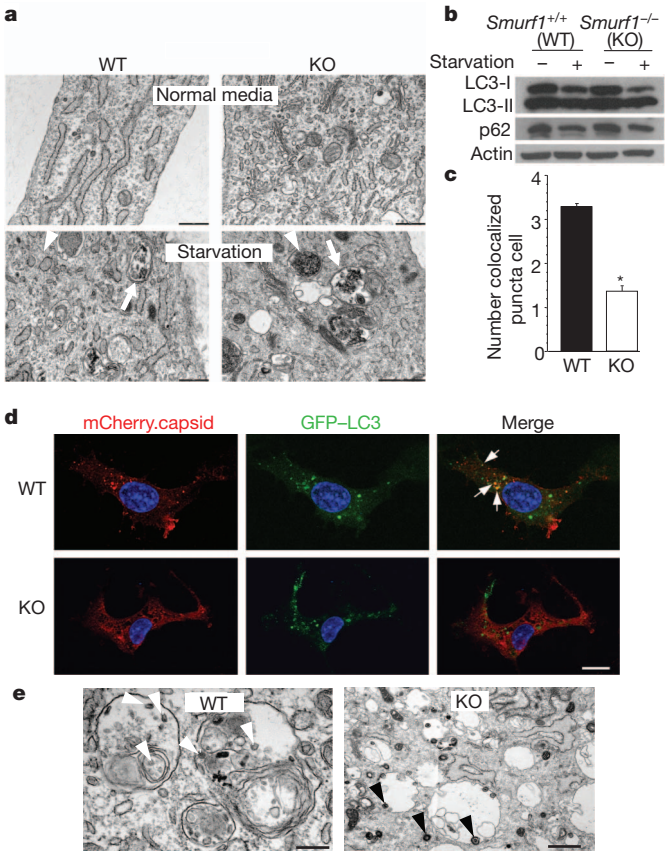

Figure 3 | SMURF1 functions in virophagy but not in starvation-induced autophagy. a, Electron microscopy analysis of wild-type (WT) and *Smurf1*$^{-/-}$ (KO) MEFs grown in normal media or EBSS (starvation) for 4 h. Arrowheads, representative autophagosomes; arrows, representative autolysosomes. Scale bars, 500 nm. **b**, Western blot analyses of LC3-I/II (non-lipidated and lipidated forms of MAP1LC3, respectively) and p62 levels in MEFs of indicated genotype. **c**, Quantification of colocalization of SIN/mCherry.capsid and GFP–LC3 in indicated MEFs 16 h after SIN/mCherry.capsid/GFP–LC3 infection. Data shown represent mean ± s.e.m. number of colocalized red and green puncta per cell for 50 cells per well in triplicate samples. $*P < 0.001$ against wild-type, Student's *t*-test. **d**, Representative confocal micrographs of images used for quantification in **c**. Arrows, colocalized red and green puncta. Scale bar, 15 μm. **e**, Representative electron microscopy images of indicated MEFs infected with HSV-1 (strain 17termA). White arrowheads, partially degraded viral nucleocapsids inside autolysosomes; black arrowheads, intact viral nucleocapsids inside viral vesicles. Scale bar, 0.5 μm. For **a**–**e**, similar results were obtained in 3–5 independent experiments.

targeting to autophagosomes and degradation through a proteasome-independent pathway, and SMURF1-dependent degradation of SIN capsid promotes cell survival.

To determine whether SMURF1 is required for the autophagic targeting of other viruses, we performed electron microscopy of wild-type and *Smurf1*$^{-/-}$ MEFs infected with a mutant strain of herpes simplex virus type 1 harbouring a deletion of ICP34.5, a potent inhibitor of viral autophagy[16–18] (Fig. 3e). As reported[17], the majority of cytoplasmic HSV-1 virions in wild-type MEFs were inside autolysosomal structures and appeared partially degraded. In contrast, in *Smurf1*$^{-/-}$ MEFs, the majority of cytoplasmic HSV-1 virions were inside single-membraned vesicles involved in HSV-1 cytoplasmic egress and had an intact structure. This lack of autophagic targeting of HSV-1 in *Smurf1*$^{-/-}$ MEFs was not due to a general defect in autophagy, because HSV-1 infection induced autophagy similarly in *Smurf1*$^{-/-}$ and wild-type MEFs (Supplementary Fig. 6b). Thus, SMURF1 is required for the autophagic targeting of both a positive-strand RNA (Sindbis) and a double-stranded DNA (herpes simplex) virus.

Next, we examined the role of SMURF1 in mitophagy. In HeLa cells, all four *SMURF1* siRNAs decreased SMURF1 protein expression (Supplementary Fig. 8a) and inhibited Parkin-mediated CCCP-induced mitophagy as effectively as an siRNA targeting *p62*, a mediator of mitophagy in some previous reports[19,20], and siRNA targeted against the essential autophagy gene, *ATG7* (Supplementary Fig. 8b, c). The magnitude of each individual siRNA's effect on SMURF1 protein expression knockdown correlated with the magnitude of inhibition of Parkin-mediated autophagy. Therefore, in the mitophagy confirmation screen, two of the *SMURF1* siRNAs were probably false negatives; indeed, the number of Parkin-expressing cells in wells treated with these siRNAs was low (data not shown), precluding meaningful statistical analyses. A similar finding was true in the viral colocalization screen.

We further examined the role of SMURF1 in mitophagy by assessing mitochondrial clearance in CCCP-treated *Smurf1*$^{-/-}$ MEFs. Unlike in HeLa cells, Parkin overexpression did not promote mitophagy in MEFs of either genotype (data not shown). However, 25–30% of MEFs treated with 10 μM CCCP showed changes in mitochondrial morphology. In wild-type MEFs with damaged mitochondria (swollen or fragmented appearance), partial mitochondrial clearance occurred with compaction of the remaining mitochondria around the nucleus (Fig. 4a). In contrast, in *Smurf1*$^{-/-}$ cells with damaged mitochondria, virtually no mitochondrial clearance occurred and there was diffuse accumulation of fragmented mitochondria throughout the cytoplasm (Fig. 4a, arrows). This phenotypic difference was confirmed using two independent methods of quantification, including assessment of the total percentage of CCCP-treated cells that displayed diffuse

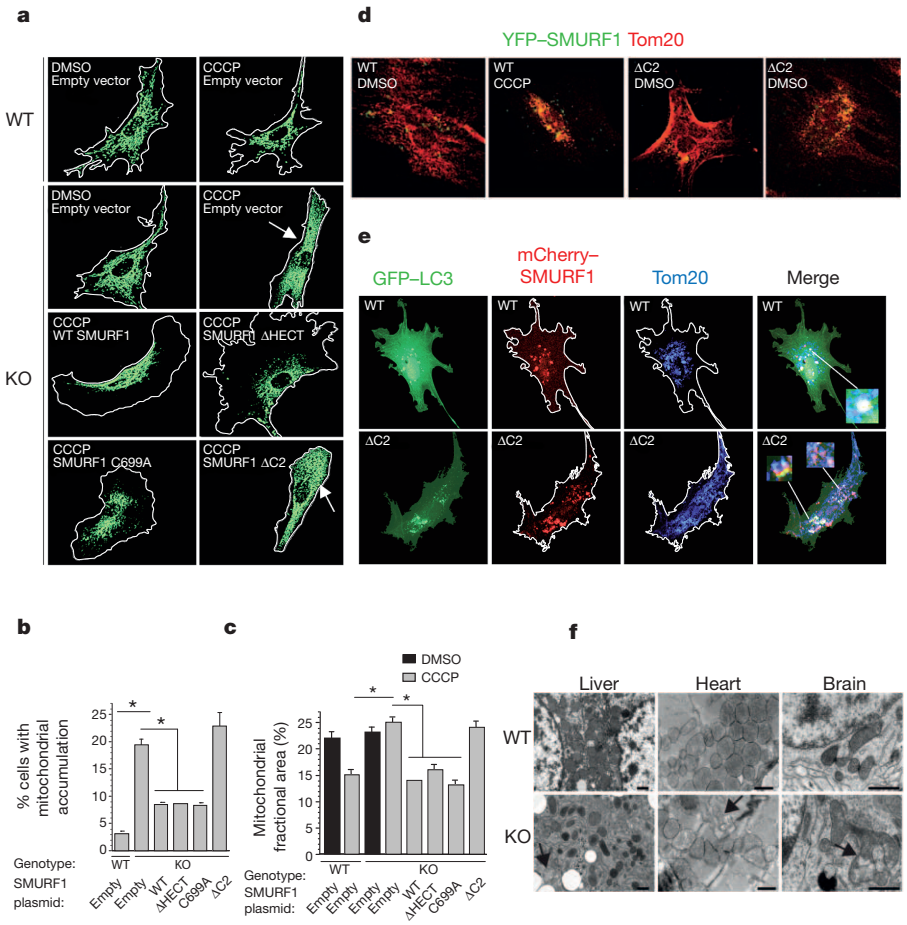

Figure 4 | SMURF1 functions in mitophagy. **a**, Representative mitochondrial morphology in *Smurf1*$^{+/+}$ (wild-type) and *Smurf1*$^{-/-}$ (KO) MEFs transfected with indicated construct and treated with DMSO or 10 μM CCCP for 24 h. **b**, Quantification of percentage of total cells with a diffuse accumulation of abnormal fragmented mitochondria and lack of mitochondrial clearance. Results shown represent combined data from 3–5 experiments per condition with triplicate wells (of at least 100 cells per well) analysed for each condition per experiment. Shown are mean ± s.e.m. for average values from each experiment. Similar results were observed in each independent experiment. *$P < 0.001$, Student's *t*-test. **c**, Measurement of mitochondrial fractional area (percentage of total cellular area) in MEFs treated as in **a**. Results shown represent mean ± s.e.m. for 50 cells per condition. **d**, Representative confocal micrographs of KO MEFs transfected with YFP–SMURF1 wild-type or YFP–SMURF1ΔC2 (ΔC2) and treated for 4 h with DMSO or CCCP. **e**, Representative confocal micrographs of KO MEFs transfected with GFP–LC3 and wild-type mCherry–SMURF1 (WT) or mCherry–SMURF1ΔC2 (ΔC2) and treated for 4 h with CCCP. Inset, upper right, formation of completed autophagosome around a damaged mitochondrion associated with wild-type SMURF1; insets, lower right, incomplete autophagosomes or absence of LC3 signal around mitochondria associated with SMURF1ΔC2. See also Supplementary Figs 10 and 11 for enlarged images. **f**, Representative electron microscopy images of indicated tissues from 10-month-old *Smurf1*$^{+/+}$ (WT) or *Smurf1*$^{-/-}$ (KO) mice. Arrows, representative abnormal mitochondria. Scale bars, 1 μm. Similar abnormalities were observed throughout entire electron microscopy tissue section for each mouse and in tissue samples from three different mice for each genotype.

accumulation of abnormal mitochondria (Fig. 4b) and the measurement of fractional mitochondrial surface area per cell (Fig. 4c).

To evaluate the mechanism of action of SMURF1, we compared the effects of wild-type and mutant SMURF1 expression plasmids on rescue of selective autophagy in *Smurf1*$^{-/-}$ MEFs (Fig. 4a–c). We focused on mitophagy rather than SIN capsid virophagy because of the resistance of MEFs to SIN infection after plasmid transfection. The defect in mitophagy in *Smurf1*$^{-/-}$ MEFs was partially rescued by wild-type SMURF1 transfection. SMURF1ΔHECT[21], lacking the HECT domain that catalyses ubiquitin ligation onto target proteins, or SMURF1(C699A)[21], a catalytically inactive point mutant, rescued the mitochondrial clearance defect as efficiently as wild-type SMURF1. Thus, in addition to its known role in targeting proteins for proteasomal degradation via ubiquitination, SMURF1 has a ubiquitin ligase activity-independent function in mediating the selective degradation of damaged mitochondria.

In contrast, a SMURF1 mutant lacking the C2 domain, SMURF1ΔC2, was completely defective in mitophagy rescue in CCCP-treated *Smurf1*$^{-/-}$ MEFs (Fig. 4a–c), despite similar levels of expression as transfected wild-type SMURF1 (Supplementary Fig. 9a). The C2 domain of SMURF1 was not required for SMURF1 co-immunoprecipitation with p62 (Supplementary Fig. 9b), indicating that SMURF1 does not function in selective autophagy by recruiting p62. C2 domains (including those of protein kinase C and SMURF1) bind membrane phospholipids and function in protein targeting to the plasma membrane and/or membrane subcellular compartments[22,23]. This raised the possibility that SMURF1 might function in the targeting of selective autophagy cargo through interaction with the nascent autophagosome membrane.

To investigate this possibility, we examined the subcellular localization of wild-type SMURF1 and SMURF1ΔC2 with damaged mitochondria and autophagosomes (Fig. 4d). In *Smurf1*$^{-/-}$ MEFs transfected with wild-type, yellow fluorescent protein-conjugated YFP–SMURF1, CCCP treatment induced the colocalization of YFP–SMURF1 with damaged mitochondria. In *Smurf1*$^{-/-}$ MEFs transfected with YFP–SMURF1ΔC2, increased numbers of fragmented and swollen mitochondria were observed in basal conditions and these increased further upon CCCP treatment. These abnormal mitochondria colocalized with YFP–SMURF1ΔC2, whereas normal reticular-appearing mitochondria rarely colocalized with YFP–SMURF1ΔC2. YFP–SMURF1(C699A) displayed the same subcellular staining pattern as wild-type YFP–SMURF1 (data not shown). Thus, SMURF1 colocalizes with damaged mitochondria in a C2 domain-independent manner.

We next determined whether the C2 domain of SMURF1 was required for the colocalization of damaged mitochondria with autophagosomes (Fig. 4e and Supplementary Figs 10 and 11). In cells expressing wild-type mCherry–SMURF1, mitochondria were mostly compacted around the nucleus, and numerous autophagosomes were observed surrounding structures that labelled positive for both mCherry–SMURF1 and the mitochondrial marker, Tom20 (also known as TOMM20). In contrast, in cells expressing mCherry–SMURF1ΔC2, mCherry–SMURF1ΔC2- and Tom20-postive mitochondria were rarely found inside autophagosomes. In many regions, GFP–LC3-positive linear or cup-shaped structures were observed near mCherry–SMURF1ΔC2-positive mitochondria, but complete autophagosomes surrounding these mitochondria could not be detected. Thus, the C2 domain of SMURF1 is

not required for its targeting to damaged mitochondria, but is required for damaged mitochondria to be normally engulfed by autophagosomes. It is not yet known whether this requirement reflects a direct role for the C2 domain in binding to autophagosomal membrane phospholipids or is a more indirect consequence of other, as-yet-undescribed, effects of the C2 domain in mitophagy.

To investigate whether SMURF1 may function in selective autophagy *in vivo*, we performed electron microscopy analyses of cerebellum, liver and hearts of 10-month-old wild-type and *Smurf1*$^{-/-}$ mice[21]. In all three organs, *Smurf1*$^{-/-}$ mice showed an accumulation of abnormal mitochondria that were swollen, fragmented, and/or contained abnormal cristae (Fig. 4f). This phenotype is consistent with a defect in mitophagy and mitochondrial quality control; however, we cannot rule out unknown triggers of mitochondrial damage in these animals. In the livers of *Smurf1*$^{-/-}$ mice, mitochondria were spatially disorganized and surrounded by networks of dilated endoplasmic reticulum, perhaps reflecting a defect in mitochondrial targeting by isolation membranes (which are believed to originate from the endoplasmic reticulum[1]) and/or a defect in selective autophagy of the endoplasmic reticulum. There was a marked accumulation of lipid droplets in the livers of *Smurf1*$^{-/-}$ mice (Supplementary Fig. 12a), which may be consistent with selective degradation of lipid droplets by autophagy (lipophagy) in hepatocytes[24]. Furthermore, the granule cell layer of the cerebellum and cardiomyocytes of *Smurf1*$^{-/-}$ mice had increased numbers of p62 aggregates (Supplementary Fig. 12b). Unlike findings in brains and hearts of mice lacking core autophagy genes[25], p62 aggregate accumulation in these tissues was not associated with ubiquitin accumulation. This is consistent with a role for SMURF1 in selective autophagy but not in the form of basal autophagy that is involved in protein quality control[25].

Together, our data in *Smurf1*$^{-/-}$ MEFs and in *Smurf1*$^{-/-}$ mice suggest a crucial function for SMURF1 in selective autophagy, including in the autophagic targeting of genetically distinct viruses, in the autophagic targeting of mitochondria and, more speculatively, in the potential autophagic targeting of other cellular targets such as hepatic lipid droplets and endoplasmic reticulum. The mechanism by which SMURF1 functions in selective autophagy is independent of its E3 ubiquitin ligase activity, but rather involves its C2 membrane-targeting domain. We propose that the C2 domain of SMURF1 may participate in the delivery of selective autophagic substrates to the nascent autophagosome. Thus, SMURF1 has parallel functions in two distinct cellular degradation pathways, targeting specific proteins for degradation by the ubiquitin-proteasomal pathway[15] (via its E3 ubiquitin ligase activity) and targeting selective cargo for degradation by the autophagy pathway (via its C2 domain).

Our findings in *Smurf1*$^{-/-}$ MEFs and mice illustrate that our high-content image-based genome-wide screen successfully reveals novel candidate determinants of selective autophagy. More broadly, the identification of a set of 96 genes that may dually function in viral autophagy and mitophagy (but not in basal autophagy) suggests the existence of a common molecular network for targeting diverse unwanted cytoplasmic cargo to the lysosome. This network identification provides a basis for a more global understanding of the mechanisms involved in selective autophagy.

METHODS SUMMARY

High-content image-based genome-wide siRNA screen. A genome-wide siRNA library (Dharmacon) containing 21,125 SMART pools was used for reverse transfection of HeLa/GFP–LC3 cells, followed by infection with SIN/mCherry.capsid virus, high content imaging using a Pathway855 automated microscope (BD Biosciences), quantitative image analysis, statistical analysis, and bioinformatic analysis as described in Supplementary Information. Primary hits were evaluated in three confirmation/secondary screens using the four individual siRNAs from each pool, including a screen for viral capsid/autophagosome colocalization, cell survival during SIN infection, and Parkin-induced mitophagy.

Functional analyses of SMURF1. See Supplementary Information.

Received 6 September 2010; accepted 7 September 2011.
Published online 23 October 2011.

1. Levine, B., Mizushima, N. & Virgin, H. W. Autophagy in immunity and inflammation. *Nature* **469,** 323–335 (2011).
2. Noda, N. N., Ohsumi, Y. & Inagaki, F. Atg8-family interacting motif crucial for selective autophagy. *FEBS Lett.* **584,** 1379–1385 (2010).
3. Wild, P. *et al.* Phosphorylation of the autophagy receptor optineurin restricts *Salmonella* growth. *Science* **333,** 228–233 (2011).
4. Komatsu, M. & Ichimura, Y. Selective autophagy regulates various cellular functions. *Genes Cells* **15,** 923–933 (2010).
5. Lipinski, M. M. *et al.* A genome-wide siRNA screen reveals multiple mTORC1 independent signaling pathways regulating autophagy under normal nutritional conditions. *Dev. Cell* **18,** 1041–1052 (2010).
6. Orvedahl, A. O. *et al.* Autophagy protects against Sindbis virus infection of the central nervous system. *Cell Host Microbe* **7,** 115–127 (2010).
7. Monastyrska, I., Rieter, E., Klionsky, D. J. & Reggiori, F. Multiple roles of the cytoskeleton in autophagy. *Biol. Rev. Camb. Philos. Soc.* **84,** 431–448 (2009).
8. Lee, J. Y. *et al.* HDAC6 controls autophagosome maturation essential for ubiquitin-selective quality-control autophagy. *EMBO J.* **29,** 969–980 (2010).
9. Longatti, A. & Tooze, S. A. Vesicular trafficking and autophagosome formation. *Cell Death Differ.* **16,** 956–965 (2009).
10. Nair, U. *et al.* SNARE proteins are required for macroautophagy. *Cell* **146,** 290–302 (2011).
11. Behrends, C., Sowa, M. E., Gygi, S. P. & Harper, J. W. Network organization of the human autophagy system. *Nature* **466,** 68–76 (2010).
12. Mizushima, N. The role of the Atg1/ULK1 complex in autophagy regulation. *Curr. Opin. Cell Biol.* **22,** 132–139 (2010).
13. Narendra, D., Tanaka, A., Suen, D. F. & Youle, R. J. Parkin is recruited selectively to impaired mitochondria and promotes their autophagy. *J. Cell Biol.* **183,** 795–803 (2008).
14. Pagliarini, D. J. *et al.* A mitochondrial protein compendium elucidates complex I disease biology. *Cell* **134,** 112–123 (2008).
15. Xing, L., Zhang, M. & Chen, D. Smurf control in bone cells. *J. Cell. Biochem.* **110,** 554–563 (2010).
16. Talloczy, Z. *et al.* Regulation of starvation- and virus-induced autophagy by the eIF2α kinase signaling pathway. *Proc. Natl Acad. Sci. USA* **99,** 190–195 (2002).
17. Talloczy, Z., Virgin, H. W. I. V. & Levine, B. PKR-dependent xenophagic degradation of herpes simplex virus type 1. *Autophagy* **2,** 24–29 (2006).
18. Orvedahl, A. *et al.* HSV-1 ICP34.5 confers neurovirulence by targeting the Beclin 1 autophagy protein. *Cell Host Microbe* **1,** 23–35 (2007).
19. Geisler, S. *et al.* PINK1/Parkin-mediated mitophagy is dependent on VDAC1 and p62/SQSTM1. *Nature Cell Biol.* **12,** 119–131 (2010).
20. Narendra, D., Kane, L. A., Hauser, D. N., Fearnley, I. M. & Youle, R. J. p62/SQSTM1 is required for Parkin-induced mitochondrial clustering but not mitophagy; VDAC1 is dispensable for both. *Autophagy* **6,** 1090–1106 (2010).
21. Yamashita, M. *et al.* Ubiquitin ligase Smurf1 controls osteoblast activity and bone homeostasis by targeting MEKK2 for degradation. *Cell* **121,** 101–113 (2005).
22. Cho, W. & Stahelin, R. V. Membrane binding and subcellular targeting of C2 domains. *Biochim. Biophys. Acta* **1761,** 838–849 (2006).
23. Lu, K. *et al.* Pivotal role of the C2 domain of the Smurf1 ubiquitin ligase in substrate selection. *J. Biol. Chem.* **286,** 16861–16870 (2011).
24. Singh, R. *et al.* Autophagy regulates lipid metabolism. *Nature* **458,** 1131–1135 (2009).
25. Mizushima, N. & Levine, B. Autophagy in mammalian development and differentiation. *Nature Cell Biol.* **12,** 823–830 (2010).

Supplementary Information is linked to the online version of the paper at www.nature.com/nature.

Acknowledgements We thank M. Vishwanath, S. Wei and B. Posner for assistance with high-throughput siRNA screening; W. Sun for information technology support; K. Scudder for assistance with image analysis algorithms; A. Diehl for expert medical illustration; V. Stollar, M. McDonald, R. Kuhn and R. Youle for helpful discussions and providing reagents; A. Bugde for assistance in the UTSW Live Cell Imaging Facility; and L. Mueller and T. Januszewski for assistance with electron microscopy. This work was supported by NIH grants AI109617 (B.L.), CA84254 (B.L.), UL1 RR024982 (G.X., Y.X.), AI062773 (R.J.X.), DK83756 (R.J.X.), DK086502 (R.J.X.) and DK043351 (R.J.X. and A.N.); NSF grant DMS-0907562 (G.X.); and the Center for Cancer Research, National Cancer Institute Intramural Research Program (Y.E.Z.).

Author Contributions A.O., R.S., M.N., M.R., J.L.W., Y.E.Z., K.L.-P., C.G. and B.L. designed the experiments. A.O., R.S., Z.Z. Q.S. and Y.T. performed the experiments. G.X., A.N., C.V.F., R.J.X. and Y.X. performed statistical and bioinformatic analyses. A.O., R.S. and B.L. wrote the manuscript. G.X. and A.N. contributed equally to the manuscript.

Author Information Reprints and permissions information is available at www.nature.com/reprints. The authors declare no competing financial interests. Readers are welcome to comment on the online version of this article at www.nature.com/nature. Correspondence and requests for materials should be addressed to B.L. (beth.levine@utsouthwestern.edu).